ELSEVIER

Journal of Alloys and Compounds 216 (1994) 123–129

Journal of ALLOYS AND COMPOUNDS

A neutron diffraction investigation of the $LaNi_5$–D phase diagram

E.H. Kisi[a,1], E. Mac A. Gray[a,*], S.J. Kennedy[b]

[a]*Faculty of Science and Technology, Griffith University, Nathan, Qld. 4111, Australia*

[b]*Neutron Scattering Section, Australian Nuclear Science and Technology Organisation, Locked Bag 1, Menai, N.S.W. 2234, Australia*

Received 15 April 1994

Abstract

Phase boundaries in the $LaNi_5$–D system determined by in situ neutron diffraction experiments have shown good agreement with those predicted from the $LaNi_5$–D pressure–composition phase diagram by intersecting extrapolated pressure plateaux and pure phase isotherms. Lattice parameter measurements show strong dilational strain in the α phase and severe compressive strain in the β phase in the two-phase region. In addition, there are systematic changes in linewidths in the two-phase region. Taken together, these provide strong evidence that the partially hydrided powder is microscopically inhomogeneous, i.e. individual micron-sized particles contain coexisting nanoscale α and β phase domains. The alternative model, consisting of a mixture of particles which are wholly α and particles which are wholly β phase, is not supported by these data. We observed hysteresis in the lattice parameters of the β phase and the linewidths of the α phase in the two-phase region, implying a fundamental asymmetry in the D absorption and desorption mechanisms.

Keywords: Neutron diffraction; Phase diagrams

1. Introduction

In metal–hydrogen (or metal–deuterium) systems, phase diagrams are usually measured as pressure–composition (P–C) isotherms during stepwise absorption and desorption of gaseous hydrogen (see Fig. 1). Because the transitions between the single-phase α or β regions and the two-phase $\alpha+\beta$ region on the P–C diagram are not sharp, the precise positions of the phase boundaries are usually taken as the intersections of linearly extrapolated single-phase isotherms with extrapolated plateaux. We will refer to this as method I. Mean field models used to describe hysteresis as a bi-stability arising from the combined effect of site potentials and H–H (or D–D) interactions suggest that the phase boundary should be located at the stationary points ($dP/d(D/M)=0$) of the single-phase α and β isotherms of an idealized P–C diagram with horizontal plateaux. In real P–C diagrams with sloping plateaux the minimum slope on the single-phase portion of the isotherms would correspond to the beginning and end of the linear parts of the plateaux. We will refer to this as method II.

In addition, whilst the $\alpha+\beta$ region is intrinsically inhomogeneous, previous experimentation has not revealed what form the inhomogeneity takes. Does each powder particle partition into small α and β regions or do whole particles transform rapidly, leaving the powder as a mixture of α and β phase particles as has been suggested in the literature [1]? These questions are intimately linked to the problem of the atomic scale origin(s) of hysteresis itself (see. e.g. Ref. [2]).

Previous neutron diffraction studies have focused on the crystal structures of the pure α [3,4] and β phases [5–7]. Furthermore, they have generally been conducted on samples loaded with D in external apparatus and transferred to the neutron diffractometer at low temperature or after some stabilization treatment. We are aware of no reports concerning the two-phase region separating the pure phases.

A neutron diffraction investigation of the complete $LaNi_5$–D phase diagram at 22 °C has been undertaken with the aim of answering or clarifying the above questions. We find that the phase boundaries determined by quantitative phase analysis (QPA) and from lattice parameter measurements are in good agreement

*Corresponding author.

[1]Present address: Department of Mechanical Engineering, University of Newcastle, Newcastle, N.S.W. 2308, Australia.

SSDI 0925-8388(94)01252-D

with those found from extrapolated α and β boundaries on pressure–composition diagrams. In addition, we have strong evidence from lattice parameters and line-broadening data that in the two-phase region α and β coexist within the same particles. Lattice parameter measurements also give us some evidence of the strains present in the phase coexistent at various D/M values along the plateaux.

2. Experimental details

$LaNi_{4.93}$, alloy #1241 from Research Chemicals, Phoenix, AZ, and Matheson deuterium (greater than 99.5% pure) were used in this work. Deuterium needs to be substituted for hydrogen in neutron-scattering experiments because of the very high incoherent scattering cross-section of the latter isotope. The sample used in this work had undergone more than 20 deuterium absorption–desorption cycles during which $LaNi_5$ fractures into a powder of 2–10 μm particles. No further powder preparation is necessary for diffraction measurements.

Pressure–composition diagrams were measured by the well-known manometric technique of preparing an aliquot of D_2 in a standard reference volume, opening a valve to the sample space and measuring the pressure decrease in the total volume so formed.

A preliminary experiment was conducted using the fixed-wavelength diffractometer MRPD [8] at the Australian Nuclear Science and Technology Organisation's reactor HIFAR. MRPD has a moderately high resolution ($FWHM_{min}=0.35°$ 2θ) over a wide range of 2θ. Neutron diffraction patterns were collected at $\lambda=1.32$ Å using an in situ apparatus consisting of a thin-walled stainless steel sample chamber attached to the manometric apparatus described above. Although much useful information was obtained, the available neutron flux was too small to achieve our aim of executing an entire pressure–composition hysteresis loop while recording diffraction patterns at many compositions.

A more complete experiment in a modified sample chamber [9] was conducted on the high intensity diffractometer POLARIS at the Rutherford–Appleton Laboratory's ISIS facility. Complete time-of-flight diffraction patterns were able to be collected in just 30 min. We waited 30 min for the system pressure to settle after each D/M increment before collecting data. Fig. 1 shows the P–C diagram recorded at the same time as the POLARIS experiment. Each P–C data point in Fig. 1 therefore also corresponds to the pressure and deuterium-to-metal atomic ratio (D/M) at which a neutron diffraction pattern was recorded.

Time-of-flight data from the low angle (low resolution) and high angle (high resolution) detector banks were converted to equivalent fixed-wavelength patterns at

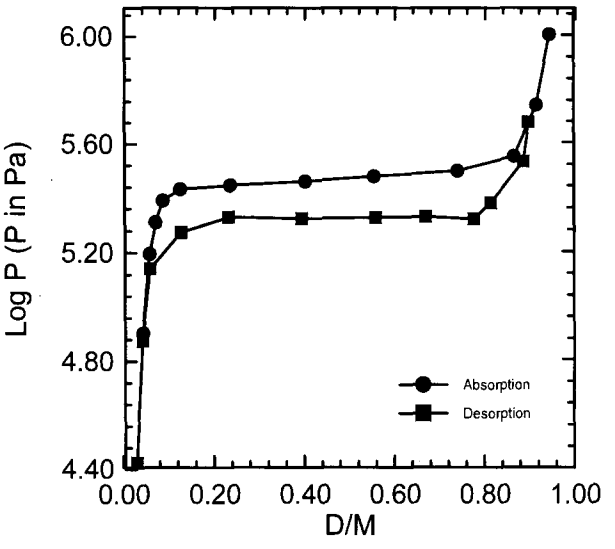

Fig. 1. Pressure–composition phase diagram for $LaNi_5$–D recorded during the in situ neutron diffraction experiment.

$\lambda=1.32$ Å so that they could be analysed using locally modified computer software (see below). A range from 12° to 130° 2θ in 0.05° steps was utilized. During the conversion, care was taken that all intensity and error information remained properly scaled so that subsequent data analysis would provide correct error estimates for the refined parameters. In the calculation of integrated intensities for such converted data the Lorentz factor is constant (constant detector angle) and the wavelength dependence was included, since each data point arises from neutrons of a different wavelength.

Diffraction patterns of activated $LaNi_5$ and $LaNi_5D_6$ exhibit strong anisotropic line broadening. The data were analysed by a modified Rietveld refinement technique which is detailed elsewhere [10]. In brief, the anisotropic line broadening is modelled as a combination of isotropic particle size broadening and anisotropic strain. The strain is zero for $\{00l\}$ reflections and maximum for $\{hk0\}$ reflections. This combination is catered for in the Rietveld calculation by allowing the a unit cell parameter to have a Gaussian distribution about its mean value. The c parameter has a discrete value. A typical Rietveld fit for the α phase pattern recorded by the low angle detector bank is shown in Fig. 2. The success of the conversion from time-of-flight to equivalent fixed-wavelength data is apparent in (i) the good visual fit in Fig. 2 and (ii) the agreement indices ($R_{wp}=4.02\%$, GOF=3.48 and $R_B=2.19\%$ for the refinement in Fig. 2). In general, data from the low angle detector bank were used, because there is little or no overlap of the low index reflections accessible there. The anisotropy of linewidth is not very obvious because of the low resolution of the low angle detector bank, but the correction is still required to fit the data correctly. The anisotropy correction was also tested on data from the high angle data bank and was in good

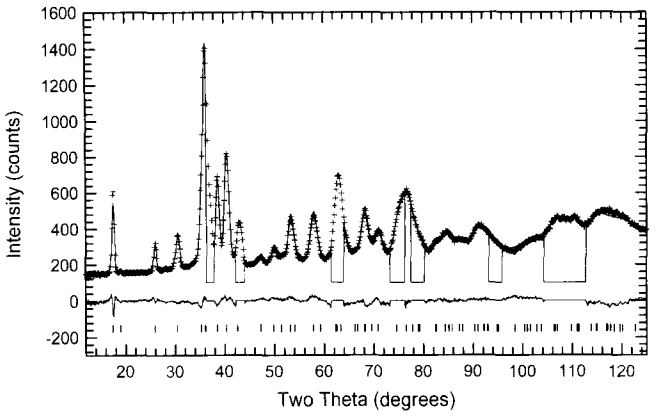

Fig. 2. Results of Rietveld refinement of the α phase data at D/M = 0. The data are shown as crosses (alternate points omitted for clarity) and the calculated profile as a solid line through them. Below are shown a difference plot on the same scale and reflection markers to indicate the peak positions.

agreement. Owing to strong preferred orientation in the diffraction lines from the stainless steel sample can, they could not be modelled correctly and were excluded from the calculations. Rietveld scale factors were used for QPA [11]. The refinements also provide lattice parameters for each phase, some structure information and linewidth parameters from which r.m.s. strains can be calculated. In the two-phase region, structural information such as atom coordinates and thermal parameters was held constant.

3. Results and discussion

Our preliminary experiment on MRPD confirmed the expected structures of the pure α and β phases in our material and indicated that phase proportions determined from the application of the lever rule to the P–C phase diagram agree with those from QPA. The results of the comprehensive POLARIS experiment are presented in detail below. The agreement indices for all refinements were in the ranges R_{wp} 3.1%–4.9% and R_B (for both phases) 1.1%–3.0% depending on the relative proportions of the phases.

3.1. Structures

An α phase model in *P6/mmm* founded on our own unpublished high resolution neutron powder diffraction was supported by this work. The best fit was obtained with deuterium in the basal plane interstitial site. This is variously quoted in the literature [3,4] as ($\frac{1}{2}$,0,0) or (0.45,0,0.11). Refinements were conducted using each of the interstitial sites of $LaNi_5$ (i.e. each of the D sites in the five-site β phase model of Percheron-Guegan et al. [7]) of which the former are but two. In each case except (0.45,0,0.11) the agreement indices (R values) were good but the occupancy of the D site was in poor agreement with the known D content of the alloy and usually negative. When the D was positioned at (0.45,0,0.11) and its coordinates were refined, the agreement indices were slightly better and the refined D occupancy agreed, within error, with that measured manometrically. The x coordinate always converged towards $\frac{1}{2}$ but oscillated about that value. From this it was inferred that the correct x value is $\frac{1}{2}$. The z coordinate is stable at 0.110(7) and in subsequent refinements the D in the α phase was fixed at (0.50,0.11). The various β phase structures postulated were tested against our data. We favour the model in P31c [5] as providing a slightly better fit than the $P6_3/mmc$ models [6,5] and markedly better than the *P6/mmm* model [7].

3.2. Quantitative phase analysis

The results of the quantitative phase analysis of POLARIS data are plotted in Fig. 3 as the percentage of β phase against D/M. Values less than 2% were considered below the detection limit in these data and are recorded as 0%. The phase quantities predicted from an application of the inverse lever rule to extrapolated phase boundaries are also shown. They are only in fair agreement, in contrast with our expectation from the preliminary experiment. The usual reasons for curved QPA plots, particularly in X-ray analysis, are microabsorption and differing extinction in the two phases (see Ref. [12]). Neither of these mechanisms can operate here, since the attenuation coefficients are nearly identical and the activated metal is heavily defected [10]. The answer lies in the newly understood inhomogeneous absorption–desorption due to poor ther-

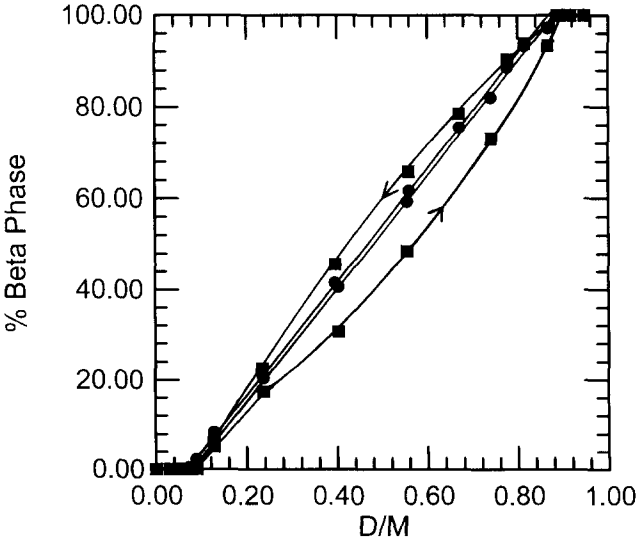

Fig. 3. Quantitative phase analysis results from Rietveld analysis of the neutron data plotted as %β phase as a function of D/M (squares) and the values predicted by an application of the inverse lever rule to the P–C diagram.

mal conductivity in the hydride bed [13,14,9], combined with a fixed-height Cd mask used to define the neutron beam. During absorption the β phase forms in greater amounts adjacent to the heat sinks located at the top and bottom of our sample cell and actively temperature controlled. Because of the 24% expansion ($\alpha \rightarrow \beta$), some of the powder is forced up out of the neutron beam into an expansion chamber in the top heat sink. Powder pushed out of the neutron beam is rich in β phase (adjacent to the heat sink) and so the amount of β phase is under-represented during absorption, until the inhomogeneity begins to even out near the end of the absorption plateau. Analogous behaviour causes under-representation of the α phase (or over-representation of the β phase in Fig. 3) during desorption. This macroscopic inhomogeneity (MI) over distances of about 2 cm is not to be confused with the local inhomogeneity on a particle-to-particle basis.

The results can still be used to locate the phase boundaries by extrapolating the (curved) QPA lines until they intersect the 0% and 100% β phase levels as demonstrated in Fig. 3. Phase boundaries determined from the P–C phase diagram by methods I and II are compared in Table 1 with those derived from the QPA results. The method of extrapolated isotherms (I) gives phase boundaries which are in much better agreement with those derived from QPA of the neutron diffraction results than method II. Had the sample remained wholly within the neutron beam during the experiment, the phase quantities measured and those predicted from method I boundaries and the inverse lever rule would also agree.

3.3. Lattice parameters

Because of the MI in the powder, D/M measured from the D_2 pressure in the apparatus is not an accurate measure of the average D/M of that part of the sample contributing to the diffraction pattern. To remedy this, a D/M scale based on the neutron diffraction QPA results (henceforth "$D/M_{neutron}$") was derived from the equation

$$D/M_{neutron} = \frac{1}{100}(\%\beta \cdot X_\beta + \%\alpha \cdot X_\alpha)$$

Table 1
Phase boundaries from two P–C methods, QPA and lattice parameters. Numbers in parentheses are the estimated errors in the last significant figure

Boundary	Method I	Method II	QPA	Lattice parameters
α–($\alpha+\beta$) absorption	0.07(1)	0.13(2)	0.08(1)	0.06(1)
α–($\alpha+\beta$) desorption	0.06(1)	0.13(2)	0.08(1)	0.06(1)
($\alpha+\beta$)–β absorption	0.88(1)	0.82(2)	0.90(2)	0.88(4)
($\alpha+\beta$)–β desorption	0.86(1)	0.80(2)	0.88(2)	0.80(2)

where X_α and X_β are the phase boundaries determined by QPA of the neutron diffraction data (i.e. column 4 of Table 1). D/M was not corrected in the single-phase regions, the effect of the MI being negligible because there is no large volume change to remove material from the neutron beam path. Use of this D/M scale to plot lattice parameters and r.m.s. strains minimizes the effect of the MI on the results.

3.3.1. The α phase

Lattice parameters for the α phase are given in Fig. 4. Phase boundaries derived from them are included in Table 1. Results for the α–($\alpha+\beta$) boundary are in agreement with method I and the QPA results.

It should be noted that the α phase unit cell parameters a and c behave differently. The larger expansion in a compared with c may merely reflect (and confirm) that the D site in α is in a densely packed part of the basal plane. Addition of extra D therefore expands a more than c.

More puzzling is the behaviour of the lattice parameters in the two-phase region. Equilibrium thermodynamics predicts that for phases in equilibrium the lattice parameters should be constant. Contrary to this, there is a marked increase in the a parameter in the two-phase region. The c parameter is more nearly constant. Two possibilities were considered.

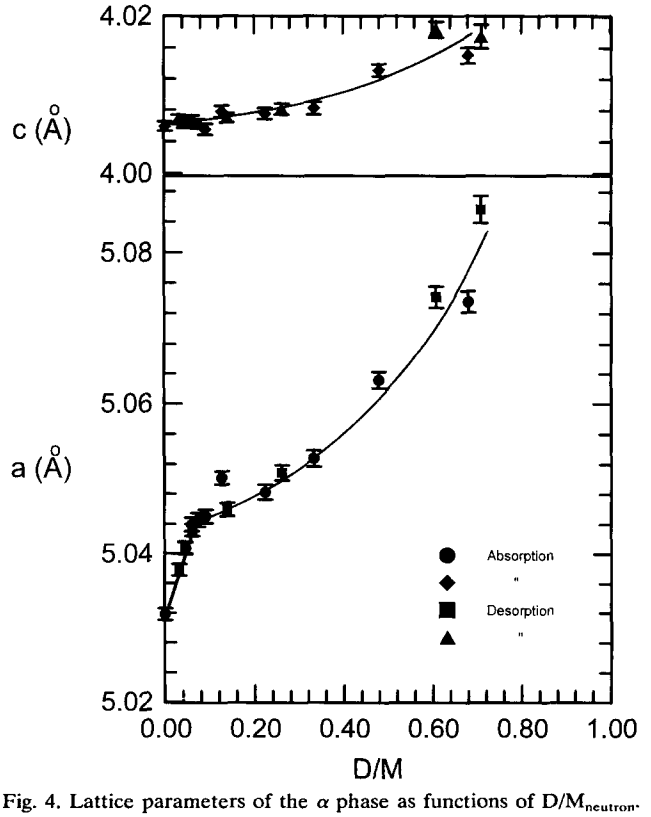

Fig. 4. Lattice parameters of the α phase as functions of $D/M_{neutron}$. Note the discontinuity at the phase boundary and the sharp rise in a in the two-phase region.

First, the pressure plateaux in $LaNi_5D_x$ are known to have slight slopes (Fig. 1). It is reasonable to expect that α phase, coexistent with β phase and in equilibrium with a gas phase at rising pressure, will absorb more D near the end of the plateau than near the beginning. The linear (low D/M) portion of Fig. 4 (*a*) gives the rate of expansion of α phase per unit of D/M. For the increase in a in the two-phase region to be explained as a consequence of plateau slope, D/M in the α phase must rise to approximately 0.23 over the length of the absorption plateau, an increase of 0.16. Examination of the P–C diagram in Fig. 1 shows that a D/M of 0.09 (or a rise of only 0.02 along the plateau) is the maximum to be expected at any pressure where α phase can exist (i.e. the highest plateaux pressure). Therefore this explanation cannot account for the observed rise.

The second explanation is that the two phases mechanically interact with each other. The expanded α phase lattice parameters are consistent with the dilational stresses expected when α coexists with β in the same powder particle, especially at low volume fraction (i.e. high D/M). Neutron diffraction estimates of the mean size of coherently scattering domains in the activated $LaNi_5$ [10] and the α and β phases (this work) are of order 300 Å. There are 10^5–10^6 such domains in each powder particle, ample for a mixture of phases to coexist.

3.3.2. The β phase

Fig. 5 shows the variation in the β phase lattice parameters with $D/M_{neutron}$. The $(\alpha+\beta)$–β phase boundaries derived from lattice parameters are in poor agreement with QPA and method I. This is discussed in Section 3.5.

Both a and c vary linearly with D/M in the single-phase β region and both decrease sharply at low D/M. It can be shown by the extrapolation technique above that the decrease in c is orders of magnitude more than that attributable to D undersaturation and sloping plateaux. The sharp decrease in the lattice parameters at low D/M is consistent with considerable compressive stress on the β phase in the two-phase region. Again this can only happen if the two phases coexist in the same powder particles. The greater change in the β phase parameters compared with the α phase parameters suggests that the bulk modulus of β is significantly lower than that of α.

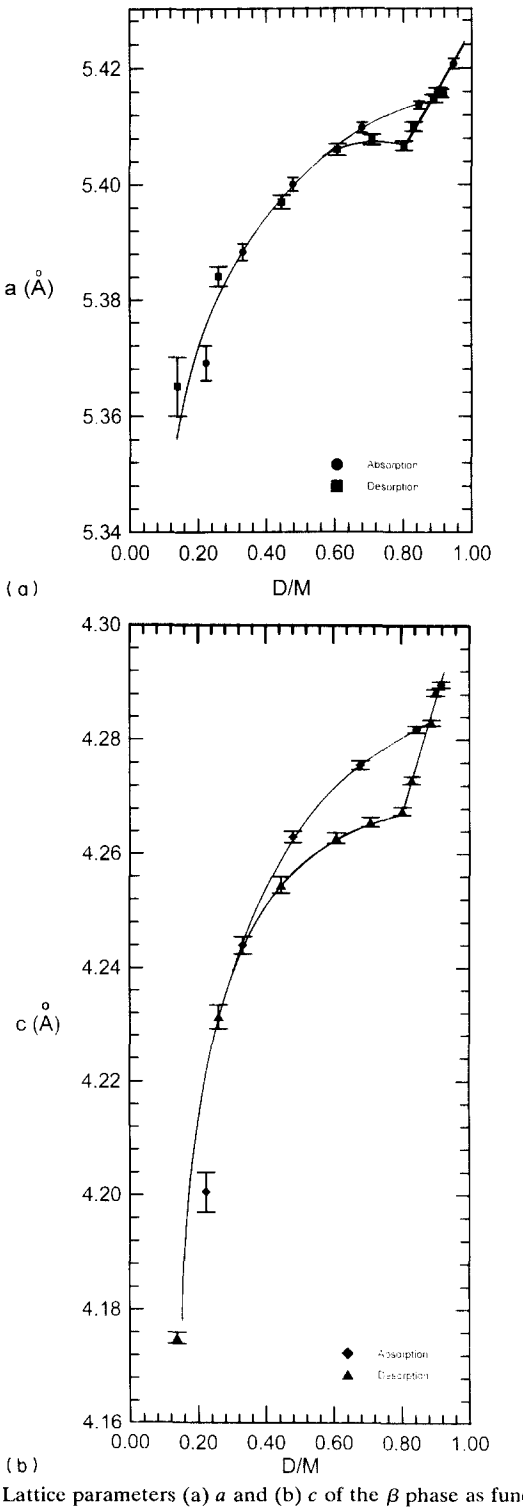

Fig. 5. Lattice parameters (a) a and (b) c of the β phase as functions of $D/M_{neutron}$. Again note the discontinuity at the phase boundary, the fall in both a and c in the two-phase region and that the parameters differ during absorption and desorption near the $(\alpha+\beta)$–β boundary.

3.4. Line broadening

The exact origins of the $\Delta a/a$ broadening are still unclear. Anisotropic broadening occurs in the activated metal and so is not caused by inhomogeneous distribution of D (over any length scale). It may be due to dislocations, stacking faults, microtwins or non-uniform strains. When interpreted on a strain model as was done previously [10], the resulting r.m.s. strains are shown in Fig. 6 as a function of $D/M_{neutron}$. The β phase generally shows broader lines than the α phase, lending weight to the notion of a reduced bulk modulus. In addition, the broadening in the β phase increases

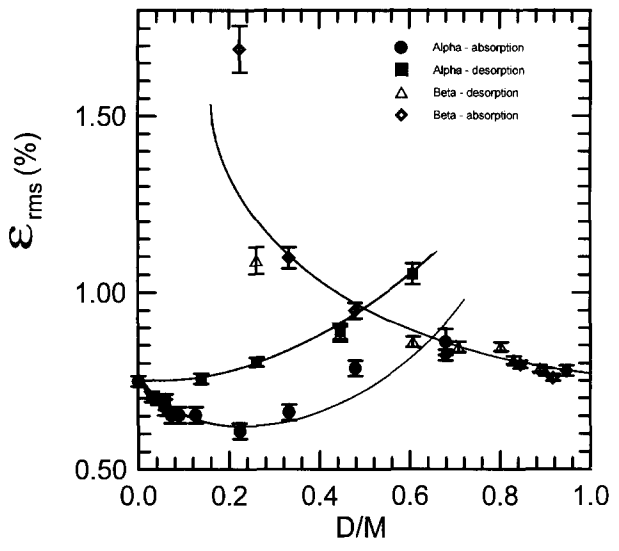

Fig. 6. Anisotropic broadening parameter for the two phases as a function of $D/M_{neutron}$, measured as r.m.s. strain in the ($hk0$) plane. Note that the two phases differ, as do the results for the α phase in absorption and in desorption.

markedly at lower D/M. The broadening in the α phase increases at high D/M. Regardless of the exact origins of the broadening, this behaviour is inconsistent with a model of the sample that consists of a mixture of separate particles which are either entirely α or entirely β phase. However, in agreement with the lattice parameter results above, it is consistent with a model in which each particle in the two-phase region consists partly of α and partly of β. Two phases with such different densities will strongly interact and we contend that the broadening behaviour and the apparent strain reflected in the lattice parameters are due to this interaction. The α phase broadening is reduced once some D is absorbed, and continues to fall during absorption in the two-phase region until $D/M \approx 0.2$. On a strain model of broadening, this indicates stress relaxation due to D absorption.

The values of mean lattice parameters $\bar{a}$ and $\bar{c}$ (and hence the mean dilational or compressive strain in the two-phase region) and the width of the strain distribution, $\Delta a/\bar{a}$, are obtained for each phase by a double-averaging process: first over the volume of (say) β phase in each diffracting particle and then over all the diffracting particles in the neutron beam. At low D/M isolated β precipitates occur in an α matrix and vice versa at high D/M. β precipitates are almost certainly nucleated heterogeneously at defects. Hence they are not spherical, the stress within them is not hydrostatic and the misfit strain field will penetrate them. Therefore the volume of strained relative to unstrained β phase will be high at low D/M, leading to a low average lattice parameter and high strain-induced line broadening. Lacking a detailed model of the interaction between the phases, no further conclusions can be drawn from the variations in $\bar{a}$, $\bar{c}$ and $\Delta a/\bar{a}$ with D/M other than that the results agree with our general expectations for interacting phases.

3.5. Hysteresis

In Fig. 5 there is an apparent hysteresis in the β phase lattice parameters in the two-phase mixture close to the $(\alpha+\beta)$–β boundary. This effect persists until approximately 10% of the sample has been converted to α phase (Fig. 3). The desorption lattice parameter curve follows the pure β slope to a low value of D/M, leading to the discrepancy in the position of the β–$(\alpha+\beta)$ phase boundary as seen in Table 1. Evidently the hysteresis is accompanied by a large undersaturation of the β phase in desorption. This may explain the usually observed gradual transition from pure β to $\alpha+\beta$ in desorption. The origin of the hysteresis is not clear, but it implies a fundamental asymmetry in the processes of α shrinking in β during absorption and α growing in β during desorption. This hysteresis cannot be a spurious result of the MI due to temperature gradients, because it is apparent through much of the two-phase region and persists when the lattice parameters are plotted against D/M derived from the neutron data themselves. No corresponding hysteresis in the α phase lattice parameters was resolved near the α–$(\alpha+\beta)$ phase boundary.

We can offer a simple model of the asymmetry as follows. In a two-phase sample where each powder particle consists of mechanically interacting domains of the α and β phases, it is reasonable to suppose the misfit strains due to the different lattice parameters will be partially accommodated by misfit dislocations. For β phase to grow, advancing the interface into α phase, these dislocations must climb positively. For α phase to grow, the dislocations climb negatively. We assume that self-interstitials play only a minor role in the climb process because of their high energies compared with vacancies. The mechanisms are then reduced to vacancy annihilation for positive climb (β growth) and vacancy production for negative climb (α growth). The former only involves the motion of pre-existing vacancies (at low energy cost) whereas the latter involves the creation of new vacancies (at higher energy cost). The growth energy for α in β should therefore be higher than for β in α, leading to undersaturation of β, as shown in Fig. 5(b).

In addition to the hysteretic behaviour of the lattice parameters, the line broadening is also hysteretic. The α phase broadening is larger in desorption than in absorption, further evidence of asymmetry in the absorption–desorption mechanism.

The weighted mean elastic volume strain

$$\frac{1}{100}\left(\%\beta\frac{\Delta V_\beta}{V_\beta}+\%\alpha\frac{\Delta V_\alpha}{V_\alpha}\right)$$

in the sample varies between 0.7% and 3.8% across the two-phase region. Assuming a bulk modulus of 200 GPa, the stored elastic strain energy in the two-phase region is therefore of order 40 MJ m^{-3} or 64 J in our sample, compared with a free-energy difference ($\frac{1}{2}RT\ln(P_{abs}/P_{des})$) of about 400 J mol^{-1} or 74 J for our sample. Thus our measurements are consistent with models of hysteresis in brittle materials as a consequence of stored elastic strain energy which is relaxed at the ends of the plateaux [15].

4. Conclusions

(1) The agreement between method I, QPA and lattice parameter measurements suggests that for the determination of phase boundaries from P–C diagrams method I is the correct one. Of the diffraction techniques, QPA is better than lattice parameters in this case, because the lattice parameters in the two-phase region are clearly not independent and constant.

(2) Lattice parameters and line-broadening behaviour lead us to conclude that in the two-phase region the two phases coexist on the nanoscale within individual micron-sized powder particles.

(3) There are some hysteretic effects in the lattice parameters and line broadening which, although not fully understood, we feel are important in the understanding of hydriding behaviour.

(4) Of the mechanically interacting phases along the pressure plateaux, β appears to have the lower elastic constants.

(5) The basis for hysteresis models relying on mechanical interaction of the coexisting phases is supported by these results.

Acknowledgments

Support is acknowledged from the Australian Research Council, the Australian Institute of Nuclear Science and Engineering and the Access to Major Facilities Fund. The help of Dr. Ron Smith and Dr. Steve Hull at ISIS is also gratefully recognized.

References

[1] S. Qian and D.O. Northwood, *Int. J. Hydrogen Energy, 17* (1992) 631–634.
[2] S. Qian and D.O. Northwood, *Int. J. Hydrogen Energy, 13* (1988) 25–36.
[3] P. Fischer, A. Furrer, G. Busch and L. Schlapbach, *Helv. Phys. Acta, 50* (1977) 421.
[4] J.L. Soubeyroux, A. Percheron-Guegan and J.C. Achard, *J. Less-Common Met., 129* (1987) 181.
[5] C. Lartigue, A. Le Bail and A. Percheron-Guegan, *J. Less-Common Met., 129* (1987) 65–76.
[6] P. Thompson, J.J. Reilly, L.M. Corliss, J.M. Hastings and R. Hempelmann, *J. Phys. F: Met. Phys., 16* (1986) 675–685.
[7] A. Percheron-Guegan, C. Lartigue, J.C. Achard, P. Germi and F. Tasset, *J. Less-Common Met., 74* (1980) 1–12.
[8] S.J. Kennedy and R.L. Davis, *Nucl. Instrum. Methods Phys. Res.*, in preparation.
[9] E.H. Kisi and E. Mac A. Gray, *J. Alloys Comp.*, in press.
[10] E.H. Kisi, C.E. Buckley and E. Mac A. Gray, *J. Alloys Comp., 185* (1992) 369–384.
[11] R.J. Hill and C.J. Howard, *J. Appl. Crystallogr., 20* (1987) 467–474.
[12] B.D. Cullity, *Elements of X-ray Diffraction*, Addison-Wesley, Reading, MA, 2nd edn., 1978.
[13] M. Pons and P. Dantzer, *Z. Phys. Chem.*, Vol. 183, in press.
[14] E. Mac A. Gray, C.E. Buckley and E.H. Kisi, *J. Alloys Comp., 215* (1994) 201.
[15] S. Qian and D.O. Northwood, *Int. J. Hydrogen Energy, 15* (1990) 649–659, and references cited therein.